CRYSTAL GROWTH & DESIGN
2007
VOL. 7, NO. 12
2460–2466

# Crystallization and Characterization of a New Magnesium Sulfate Hydrate $MgSO_4 \cdot 11H_2O$

F. Elif Genceli,*,† Martin Lutz,‡ Anthony L. Spek,‡ and Geert-Jan Witkamp†

*Process Equipment, P & E Department, Delft University of Technology, Leeghwaterstraat 44, 2628 CA Delft, The Netherlands, and Crystal and Structural Chemistry, Bijvoet Center for Biomolecular Research, Utrecht University, Padualaan 8, 3584 CH Utrecht, The Netherlands*

*Received November 9, 2006; Revised Manuscript Received July 30, 2007*

**ABSTRACT:** The $MgSO_4$ crystal hydrate formed below approximately 0 °C was proven to be the undecahydrate, $MgSO_4 \cdot 11H_2O$ (meridianiite) instead of the reported dodecahydrate $MgSO_4 \cdot 12H_2O$. The crystals were grown from solution by eutectic freeze and by cooling crystallization. The crystal structure analysis and the molecular arrangement of these crystals were determined using single crystal X-ray diffraction (XRD). Reflections were measured at a temperature of 110(2) K. The structure is triclinic with space group $P\bar{1}$ (No. 2). The crystal is a colorless block with the following parameters F.W. = 318.55, 0.54 × 0.24 × 0.18 $mm^3$, $a$ = 6.72548(7) Å, $b$ = 6.77937(14) Å, $c$ = 17.2898(5) Å, $\alpha$ = 88.255(1)°, $\beta$ = 89.478(2)°, $\gamma$ = 62.598(1)°, $V$ = 699.54(3) $Å^3$, $Z$ = 2, $D_{calc}$ = 1.512 $g/cm^3$, $\mu$ = 0.343 $mm^{-1}$. Raman spectroscopy was used for characterizing $MgSO_4 \cdot 11H_2O$ and for comparing the vibrational spectra with the $MgSO_4 \cdot 7H_2O$ salt. Between the two salts, there are significant differences mainly in the type of interactions of water with sulfate groups in the lattice, in view of the different O−H stretching vibrations, as well as sulfate, O−H···O (sulfate) and O−Mg−O bands vibrational modes. Thermogravimetric analysis confirmed the stochiometry of the $MgSO_4 \cdot 11H_2O$ salt. Additionally, the Miller indices of the major faces of $MgSO_4 \cdot 11H_2O$ crystals were defined.

## Introduction

The $MgSO_4$-$H_2O$ system is not only of industrial interest but is also a commonly used model system for crystallization investigations. $MgSO_4$ crystallizes in a large number of different hydrated forms at different working concentrations and temperatures.[1–5] In this paper, we prove that the magnesium sulfate salt formed at low temperatures is described by the formula $MgSO_4 \cdot 11H_2O$, the commonly reported $MgSO_4 \cdot 12H_2O$ being incorrect. We also present the synthesis and structure of $MgSO_4 \cdot 11H_2O$ crystals. We have developed the eutectic freeze crystallization (EFC) technique as a production method for various salts, including magnesium sulfate from industrial solutions.[6,7] EFC is a promising technique for processing waste and process streams of mixed aqueous electrolyte/organic solutions, yielding highly pure water and salt. Single crystals synthesized by EFC and cooling crystallization methods were characterized using single crystal X-ray diffraction (XRD).

According to the phase diagram of the $MgSO_4$-$H_2O$ system, $MgSO_4 \cdot 12H_2O$ (magnesium sulfate dodecahydrate) is the stable form around the eutectic point (concentration 17.3–21.4%-w $MgSO_4$ and temperature between −3.9 and 1.8 °C).[1,8–13]

The low-temperature $MgSO_4$ hydrate crystal form (which we now know to have been $MgSO_4 \cdot 11H_2O$, the undecahydrate) was discovered by Carl Julius Fritzsche in 1837.[14] Observing the crystallization behavior of a magnesium solution left outside in winter, he realized that at temperatures lower than 0 °C, small, whitish agglomerated or large transparent crystals occur, which are different from epsomite ($MgSO_4 \cdot 7H_2O$) crystals. Fritzsche mentioned that those crystals transform into $MgSO_4 \cdot 7H_2O$ at temperatures above 0 °C. For defining the water content of the new magnesium sulfate salt, he dried a single salt first with a blotting paper and then with either a flame or air drying in cold weather. From the mass balance, he proposed that the crystal has either 12 or 11 water molecules and by repeating the experiments he concluded (erroneously) that the crystals are in the form of $MgSO_4 \cdot 12H_2O$.

Frederick Cottrell, whose work had been published by Van't Hoff et al. in 1901, established the eutectic point of ice−undecahydrate at −3.9 °C and the peritectic of undecahydrate−heptahydrate at +1.8 °C,[15] reported as data for the dodecahydrate.

Marion et. al estimated the parameters of the Pitzer model and activity data for dodecahydrate using solubility data.[8] Pillay et al. improved Marion's model to fit more accurately their recent solubility data of $MgSO_4 \cdot 12H_2O$.[9] These data need to be recalculated given the new knowledge that it was the undecahydrate. Density and viscosity properties of $MgSO_4 \cdot 11H_2O$ have also been studied.[16,17]

We used $MgSO_4$ as a model solution while developing EFC technology and initially accepted that the salt produced at eutectic point was $MgSO_4 \cdot 12H_2O$ crystals.[6,7,18–20] The effects of the eutectic crystallizer design and the operation conditions on the salt quality considering kinetic relations for the population balance, impurity content, nucleation and growth rates were investigated before.[7,20,21] Using EFC, combining data of many experiments from industrial waste $MgSO_4$ solution in continuous scraped cooled wall crystallizers and a scraped cooled disk column crystallizer, the nucleation and crystal growth rates of $MgSO_4 \cdot 11H_2O$ salt were found to be $B = 1 \times 10^7 M_T \sigma^2$ (# $m^{-3}$ $s^{-1}$) and $G = 2 \times 10^{-5} \sigma^2$ (m $s^{-1}$) as a function of supersaturation ($\sigma$) and solid concentration ($M_T$).[7,20] Similarly in batch scraped crystallizers, the nucleation and crystal growth rates of $MgSO_4 \cdot 11H_2O$ salt were found to be best described as[20]

$$\text{nucleation rate}: \quad B = (6.5 \pm 5.0) \times 10^7 M_T^{(0.20\pm0.06)} \sigma^{(1.7\pm0.1)} \ (\#\text{m}^{-3}\ \text{s}^{-1}) \quad (1)$$

$$\text{growth rate}: \quad G_{salt} = (3.9 \pm 1.7) \times 10^{-6} \sigma^{(1.8\pm0.2)} \ (\text{m}\ \text{s}^{-1}) \quad (2)$$

The second order of the growth rate of eq 2 in supersaturation suggests a spiral growth mechanism.

* Corresponding author. E-mail: egenceli@hotmail.com; f.e.genceli@tudelft.nl. Tel.: +31 (0)15 2786605. Fax: +31 (0)15 2786975.
† Delft University of Technology.
‡ Utrecht University.

10.1021/cg060794e CCC: $37.00 
Published on Web 11/15/2007

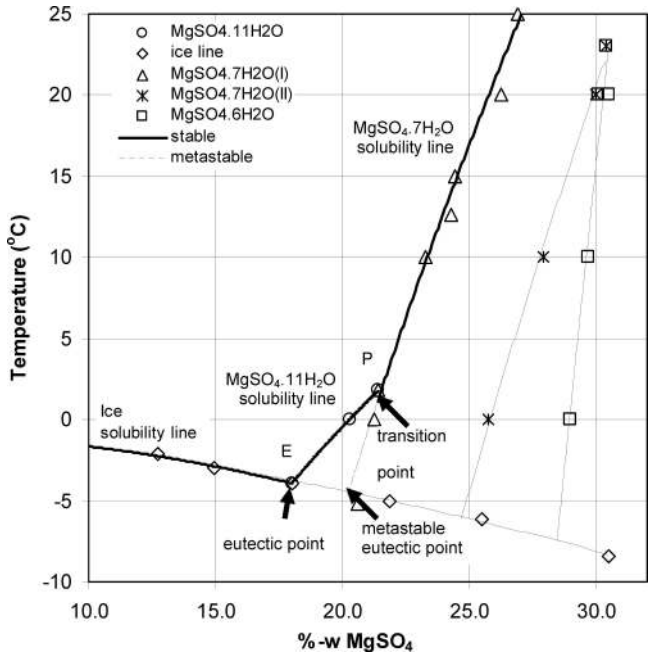


**Figure 1.** Phase diagram of the $MgSO_4 \cdot H_2O$ system. E is the eutectic point and P is the peritectic.

Considering the lack of $MgSO_4 \cdot 12H_2O$ crystal structure data, we analyzed the salt crystals produced at eutectic freeze or cooling crystallization around the eutectic point by single-crystal XRD. Surprisingly, instead of the expected $MgSO_4 \cdot 12H_2O$, a $MgSO_4 \cdot 11H_2O$ crystal structure was found. This discovery implies that $MgSO_4 \cdot 11H_2O$ has mistakenly been denoted as $MgSO_4 \cdot 12H_2O$, and since 1837, it has been named incorrectly. The purpose of this work was to correct this misconception and investigate properties of the $MgSO_4 \cdot 11H_2O$ salt such as crystallization morphology and habit, crystal structure, and Raman spectra.

## Experimental Section

**Experimental Setups.** Experiments were performed in three different set-ups.

The first setup was a 15 L, batch type, scraped cooled wall crystallizer (SCWC) designed for EFC processes. Cooling was achieved by circulating Kryo-85 cooling liquid through a thermostatic unit, Lauda RUK 90 SW. In so doing, the temperature of the cooling liquid was controlled with an accuracy of ±0.1–0.5 °C. The temperature of the $MgSO_4$ solution was measured using an ASL F250 precision thermometer connected to a PT-100 temperature sensor with an accuracy of ±0.01 °C and a resolution of 0.001 °C. More detailed description of the setup is given elsewhere.[18]

The second setup was a 220 L, continuous type, cooled disk column crystallizer (CDCC) built in a skid mounted unit designed for EFC applications. Freezium −60 °C was used as secondary cooling medium in the cooling machine, in the cooling disks, and in the plate heat exchanger precooler. During continuous EFC operation, salt and ice were sent together with the mother liquid from the CDCC to the settler in which the gravitational separation of ice and salt occurs because of their density differences. From the settler, salt was sent to a Larox-Pannevis reciprocal tray belt filter (0.2 $m^2$ filtration area) for the separation of crystals from mother liquor. The temperature of the cooling machine was controlled with an accuracy of ±0.1–0.5 °C, whereas the temperatures of the $MgSO_4$ solution, cooling liquid inlets, and outlets were measured with PT-100 temperature sensors with an accuracy of ±0.01 °C and a resolution of 0.001 °C. The CDCC, cooling machine, settler, plate heat exchanger, belt filter, measuring devices (temperature sensors, flow meters, torque meter), data acquisition, and control system are described in more detail elsewhere.[19]

The third setup was a 2 L, batch type, cylindrical jacketed glass vessel located in a climate room. The vessel was equipped with a three-leg scraper to prevent ice and scaling at the wall as to provide mixing. Cooling was achieved by circulating Kryo-51 coolant from a Lauda RK 8 KP bath through the cylinder jacket, with similar accuracies as for the setup described first above. The temperature of the climate room was regulated simultaneously with the crystallizer set temperature.

**Preparation of Solutions.** 18–20%-w $MgSO_4$ solutions, prepared with 99.99%-w $MgSO_4 \cdot 7H_2O$ (J. T. Baker) and ultrapure water of 18.2 mΩ were used in the first and third experimental setups.

In the second experimental setup, industrial magnesium sulfate solution from ex-flue gas desulphurization was used. It initially contained 17–19%-w $MgSO_4$ with the following major impurities in ppm (mg/kg) level: 300 ± 60 ppm Ca, 550 ± 100 ppm K, 70 ± 5 ppm In, 60 ± 10 ppm Na, 60 ± 8 ppm Zn, 50 ± 10 Co, 30 ± 10 ppm Mn, 20 ± 10 ppm Mo, 9 ± 2 ppm B, 4 ± 2 ppm Ni, 25 ± 10 ppm P, 10 ± 5 ppm Pb.

The magnesium sulfate concentrations of the solutions were measured offline using picnometer density measurements with an error of ±0.15%-w. Inductively coupled plasma atomic emission spectrometry (ICP-AES) and ion chromatography were used to measure the cations and anions concentrations in the mother liquor and in the crystals with an error of ±2.5%.

**Experimental Procedures. Experimental Setups.** Unseeded batch crystallization experiments in the first and third setups were started stabilizing the solution at 10 °C for 2 h. The mixing rate was 80 rpm. A cooling rate of 4 °C/h was applied until a temperature jump due to exothermic formation of the salt crystals was detected. When crystallization occurred, the coolant temperature was kept constant. After 10–15 min, a natural cooling profile was started. Natural cooling profiles were achieved by immediately cooling down the coolant medium to a certain constant temperature and letting the crystallizer respond. Every 30 min, salt samples were collected with a precooled syringe from the bottom outlets of the crystallizer. All salt samples were directly vacuum filtered using a jacket-cooled filter. The data from the temperature sensors were collected every 20 s and were recorded with Laboratory View.

In the second setup, similar to the previous ones, first nucleation was allowed to occur in batch mode by supercooling without seeding. Reaching eutectic conditions, two products (ice and salt crystals) were formed inside the crystallizer. When ice and salt crystals reached ≈200 and 250 $\mu$m mean diameter size, the crystallizer was switched to continuous operation. $MgSO_4$ feed solution was passed through the precooler and fed to the crystallizer. Inside the crystallizer, the residence time was varied between 15 min to 1 h, with the coolant set temperature set between −10 to −14 °C. The slurries (ice, salt, and solution at eutectic composition and temperature) leaving the crystallizer were fed to the settler for gravitational separation. From the settler, the bottom flow (salt and solution) was pumped to the belt filter for filtering off the mother liquor. Salt samples from the crystallizer and settling tank were taken into a precooled beaker and immediately vacuum filtered using a jacket-cooled filter. Salt samples from the belt filter were also collected after filtration.

**Picturing and Salt Preserving.** Salt samples from each setup were observed under a Leica WILD M10 stereomicroscope equipped with a Nikon Coolpix 4500 camera.

The salt crystals collected from three different setups were preserved well isolated at −20 °C for the structure determination, as they dissolve above 1.8 °C and recrystallize into the $MgSO_4 \cdot 7H_2O$ (epsomite) form.

**XRD Measurements.** A total of 40 989 reflections were measured at a temperature of 110(2) K up to a resolution of $(\sin \theta/\lambda)_{max} = 0.90$ $Å^{-1}$ on a Nonius KappaCCD diffractometer with rotating anode and graphite monochromator ($\lambda = 0.71073$ Å). The intensities were obtained with Eval14[24] using an accurate description of the crystal form and the diffraction geometry. An absorption correction based on multiple measured reflections was applied[25] (0.83–0.94 correction range). 8564 reflections were unique ($R_{int} = 0.019$). The structure was solved with Direct Methods[22] and refined with SHELXL-97[23] on $F^2$ of all reflections. Non-hydrogen atoms were refined freely with anisotropic displacement parameters. All hydrogen atoms were located in the difference Fourier map and refined freely with isotropic displacement parameters. 245 parameters were refined with no restraints. $R_1/wR_2$ [$I > 2\sigma(I)$]: 0.0222/0.0545. $R_1/wR_2$ [all reflections]: 0.0313/0.0577. $S = 1.084$. The residual electron density is between −0.43 and 0.40 e/$Å^3$.

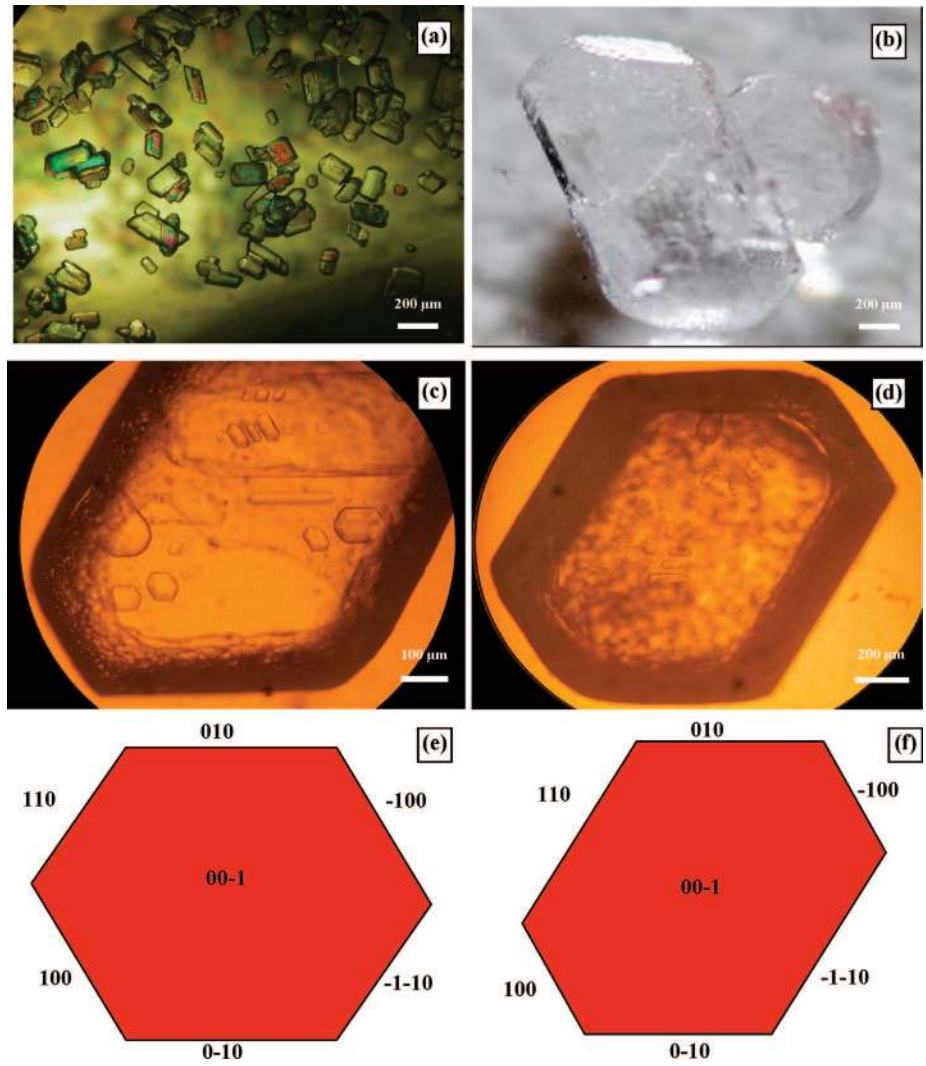


**Figure 2.** (a, b, d) Optical images of $MgSO_4 \cdot 11H_2O$. (c) Mother liquor inclusions (negative crystals) in a $MgSO_4 \cdot 11H_2O$ crystal. (e) The predicted BFDH morphology of $MgSO_4 \cdot 11H_2O$. (f) The suggested face indexing of the crystal in panel d.

Geometry calculations, drawings, and checking for higher symmetry were performed with the PLATON package.[26]

**Thermogravimetric Analysis.** Thermogravimetric analysis (TGA) of the crystal was done with a SDT 2960 (TA Instruments) with a temperature accuracy and precision of ±1 °C and ±0.5 °C, respectively, and a weight sensitivity of 0.1 μg and weight accuracy of ± 1%. TGA was carried out in helium atmosphere (with a purge rate of 100 mL/min) at a heating rate of 5 °C/min from 27 to 300 °C.

**Micro Raman Spectroscopy.** Raman spectroscopy was applied for characterization of the $MgSO_4 \cdot 11H_2O$ crystals. A Renishaw Ramanscope system 2000, equipped with a 20 mW $Ar^+$ laser ($\lambda$ = 514 nm) was used to record Raman spectra. A Leica DMLM PL Fluotar L50x/0.55 microscope was used to determine the analyzed surface of the sample. The spectral resolution was ~1 $cm^{-1}$ within the range of 100–4000 $cm^{-1}$. To investigate the sample at low temperature preventing recrystallization into $MgSO_4 \cdot 7H_2O$, $MgSO_4 \cdot 11H_2O$ crystals were kept inside an insulating vessel filled with frozen carbon dioxide prior to the measurements. A Linkam THM600 flow cell was used for the measurement below the freezing point. The cell was precooled by circulating ethylene glycol, which was set at −10 °C and by placing frozen carbon dioxide (dry ice) inside the cell. After substantial precooling of the cell, the sample was placed inside and the spectra were recorded. At ambient temperature, that is, 20 °C, the spectra of $MgSO_4 \cdot 7H_2O$ crystals were also measured for comparison. Crystals in the range of 100–4000 $cm^{-1}$ were analyzed by continuous extended scanning, with a detection time of 100 s.

## Results and Discussion

**The Crystals.** Salt samples, crystallized using pure and industrial magnesium sulfate solutions, were collected from three different crystallizer setups (running either batch or continuous mode) and from the belt filter. The samples were produced using eutectic freeze or cooling crystallization working near the equilibrium line between E and P as shown in Figure 1.

From the photograph in Figure 2, it can be seen that the crystals are well faceted, which matches with the earlier suggested spiral crystal growth based on eq 2.

All the salt samples either directly filtered from the crystallizer or taken from the belt filter were found to be $MgSO_4 \cdot 11H_2O$ crystals.

**XRD Measurements: Crystal Structure Determination.** $[Mg(H_2O)_6](SO_4) \cdot 5H_2O$ ($MgSO_4 \cdot 11H_2O$), FW = 318.55, colorless block, 0.54 × 0.24 × 0.18 $mm^3$, triclinic, $P\bar{1}$ (No. 2), $a$ = 6.72548(7), $b$ = 6.77937(14), $c$ = 17.2898(5) Å, α = 88.255(1), $\beta$ = 89.478(2), $\gamma$ = 62.598(1)°, $V$ = 699.54(3) $Å^3$, $Z$ = 2, $D_{calc}$ = 1.512 $g/cm^3$, $\mu$ = 0.343 $mm^{-1}$.

Compound $[Mg(H_2O)_6](SO_4) \cdot 5H_2O$ crystallizes in the centrosymmetric triclinic space group $P\bar{1}$. Two magnesium atoms

**Table 1. Hydrogen Bonding Interactions in $[Mg(H_2O)_6](SO_4)\cdot 5H_2O$[a]**

| D−H···A | D−H [Å] | H···A [Å] | D···A [Å] | D−H···A [°] |
|---|---|---|---|---|
| O5−H1···O12 | 0.815(12) | 1.932(12) | 2.7416(6) | 172.5(12) |
| O5−H2···O13 | 0.797(13) | 1.926(13) | 2.7197(6) | 174.1(13) |
| O6−H3···O12$^{iii}$ | 0.831(12) | 1.957(12) | 2.7813(6) | 171.2(12) |
| O6−H4···O15 | 0.819(12) | 1.904(12) | 2.7192(6) | 173.3(11) |
| O7−H5···O14 | 0.819(12) | 1.945(12) | 2.7534(6) | 169.2(11) |
| O7−H6···O13$^{iii}$ | 0.858(13) | 1.854(13) | 2.7111(6) | 178.0(13) |
| O8−H7···O4 | 0.769(12) | 2.082(12) | 2.8472(6) | 172.9(12) |
| O8−H8···O14$^{i}$ | 0.807(12) | 2.053(12) | 2.8524(6) | 170.6(11) |
| O9−H9···O11$^{iv}$ | 0.849(12) | 1.892(12) | 2.7337(6) | 170.9(11) |
| O9−H10···O4$^{v}$ | 0.823(12) | 2.039(12) | 2.8469(6) | 166.8(11) |
| O10−H11···O11$^{ii}$ | 0.869(12) | 1.886(12) | 2.7520(6) | 174.4(11) |
| O10−H12···O4$^{vi}$ | 0.785(12) | 2.044(12) | 2.8139(6) | 166.5(11) |
| O11−H13···O2$^{iii}$ | 0.865(13) | 1.969(13) | 2.8188(6) | 167.1(12) |
| O11−H14···O1$^{vii}$ | 0.856(13) | 1.896(13) | 2.7502(6) | 176.0(12) |
| O12−H15···O6$^{viii}$ | 0.803(14) | 2.591(14) | 3.1748(6) | 130.8(12) |
| O12−H15···O7$^{viii}$ | 0.803(14) | 2.236(14) | 2.9692(6) | 151.9(13) |
| O12−H16···O3 | 0.837(12) | 1.949(12) | 2.7847(6) | 175.6(11) |
| O13−H17···O15$^{viii}$ | 0.842(13) | 1.886(13) | 2.7274(6) | 178.9(12) |
| O13−H18···O2$^{ix}$ | 0.829(13) | 1.891(13) | 2.7023(5) | 165.9(12) |
| O14−H19···O2$^{ix}$ | 0.829(13) | 1.984(13) | 2.8119(6) | 176.6(12) |
| O14−H20···O3$^{viii}$ | 0.799(12) | 2.063(12) | 2.8391(6) | 163.9(11) |
| O15−H21···O3 | 0.826(11) | 1.941(11) | 2.7464(6) | 164.6(11) |
| O15−H22···O1$^{iii}$ | 0.800(13) | 1.891(13) | 2.6775(6) | 167.2(12) |

[a] Symmetry operations: i: $1-x, 1-y, 1-z$; ii: $1-x, 1-y, -z$; iii: $-1, y, z$; iv: $x+1, y, z$; v: $2-x, 1-y, -z$; vi: $1-x, 2-y, -z$; vii: $x-1, -1, z$; viii: $1-x, 2-y, 1-z$; ix: $2-x, 1-y, 1-z$.

**Table 2. Selected Bond Kengths [Å] and Bond Angles [°] in $[Mg(H_2O)_6](SO_4)\cdot 5H_2O$**

| | | | |
|---|---|---|---|
| Mg1−O5 | 2.0383(4) | Mg1−O6 | 2.0625(4) |
| Mg1−O7 | 2.0700(4) | Mg2−O8 | 2.0701(4) |
| Mg2−O9 | 2.0510(4) | Mg2−O10 | 2.0545(4) |
| S1−O1 | 1.4648(4) | S1−O2 | 1.4827(4) |
| S1−O3 | 1.4816(4) | S1−O4 | 1.4737(4) |
| O5−Mg1−O6 | 89.989(18) | O5−Mg1−O7 | 90.791(18) |
| O6−Mg1−O7 | 89.827(17) | O8−Mg2−O9 | 87.603(17) |
| O8-Mg2-O10 | 89.945(18) | O9-Mg2-O10 | 89.346(17) |

occupy two independent inversion centers of this space group (Wyckoff positions e and h). Both magnesium atoms are octahedrally surrounded by six coordinated water molecules. Thus, the asymmetric unit of the crystal structure contains two half-molecules of $Mg(H_2O)_6$. Further, there are one sulfate molecule and five uncoordinated water molecules in the asymmetric unit. The Mg−O distances are in the range of 2.0383(4)−2.0701(4) Å, which is in the expected range for hexahydrated magnesium.[27] The cis angles range from 87.603-(17)−92.397(17)°, while all trans angles are 180° by inversion

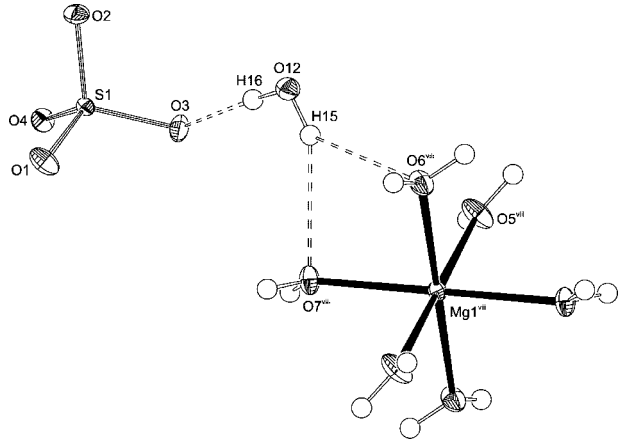


**Figure 3.** Bifurcated hydrogen bond at hydrogen atom H15. The angle sum at H15 is 357.0(18) °. Symmetry operation viii: $1-x, 2-y, 1-z$.

symmetry. Consequently, the distortions of the two independent octahedrons are very small with rms-deviations[28] from perfect $O_h$ symmetry of only 0.0219 and 0.0364, respectively.

The coordinated water molecules differ in their geometries. The angles between the least-squares plane of the water molecules O5, O8, O9, and O10 and the corresponding Mg−O vectors are 6.3, 16.6, 7.0, and 5.7°, respectively, indicating an essentially trigonal coordination mode.[29] At O6 and O7, these angles are larger with 33.5 and 23.2°, respectively, and the water molecules are thus bent. The reason for this is the intermolecular hydrogen bonding: O6 and O7 are the only coordinated water molecules which are acceptors of hydrogen bonds. The angles between the Mg−O bond and the hydrogen bonded O···H direction are 84.6(3) and 94.2(4)°, respectively.

At the measurement temperature of 110 K, the two $Mg(H_2O)_6$ octahedra differ significantly in their thermal motion. While the octahedron at Mg1 has an $R$ value of 0.080[30] and can be described as a rigid body, the $R$ value at Mg2 is 0.184 and has thus much more internal freedom. We assume that this is a consequence of the different hydrogen bond pattern of the two octahedra (vide supra).

All water molecules act as hydrogen bond donors. Hydrogen bond acceptors are all sulfate oxygens, all uncoordinated water oxygens and the coordinated water oxygens O6 and O7 (vide supra). Overall this leads to an infinite, three-dimensional hydrogen bonded network. Sulfate oxygen O1 accepts two hydrogen bonds and has a significantly shorter S−O distance than O2, O3, and O4, which accept three hydrogen bonds, respectively. Each of the uncoordinated water oxygen atoms accept two hydrogen bonds and have thus an essentially tetrahedral environment.

Hydrogen bonding interactions, and selected bond lengths [Å] and bond angles [°] in $[Mg(H_2O)_6](SO_4)\cdot 5H_2O$ are given in Tables 1 and 2, respectively. In Figure 3, a bifurcated hydrogen bond at hydrogen atom H15 is shown. The angle sum at H15 is 357.0(18)°, and the symmetry operation viii is $1-x, 2-y, 1-z$. Displacement ellipsoid plot of $[Mg(H_2O)_6](SO_4)\cdot 5H_2O$, drawn at the 50% probability level, is shown in Figure 4. Packing of $[Mg(H_2O)_6](SO_4)\cdot 5H_2O$ in the crystal is shown in Figure 5.

A comparison of the current 11-aqua $MgSO_4$ crystal structure with the 7-aqua structure ($MgSO_4\cdot 7H_2O$, epsomite) [31,32] shows that they both contain $Mg(H_2O)_6$ cations and $SO_4$ anions. The difference is the number of 5 and 1 noncoordinating $H_2O$ molecules, respectively. This leads to completely different observed hydrogen bonding systems. Nine out of the 12 hydrogen atoms of the 6 molecules that coordinate around Mg are hydrogen bonded to $SO_4$ for the 7-aqua structure where this number is only 3 out of 12 for the 11-aqua structure. This analysis can be completed with a comparison with the crystal structure of $MgSO_4\cdot 6H_2O$[33] that contains only $Mg(H_2O)_6$ cations and $SO_4$ anions. In this structure, 11 out of 12 of the hydrogen bonds are to $SO_4$.

**Thermal Analysis.** The thermogram of $MgSO_4\cdot 11H_2O$ is illustrated in Figure 6. In the TGA trace, there is a broad continuous weight loss until 225 °C, which belongs to the dehydration step by the elimination of 11 water molecules.

The average relative weight loss of eight samples (typically 25 mg) was 62.33 ± 0.38%, which corresponded to the theoretical value of 62.21% within the error limit.

**Micro Raman Spectroscopy.** The spectra of $MgSO_4\cdot 11H_2O$ and $MgSO_4\cdot 7H_2O$ are presented in Figure 7. The most significant peak is the $SO_4^{2-}$ associated symmetric stretching band at 986 $cm^{-1}$ for $MgSO_4\cdot 7H_2O$, which is shifted slightly

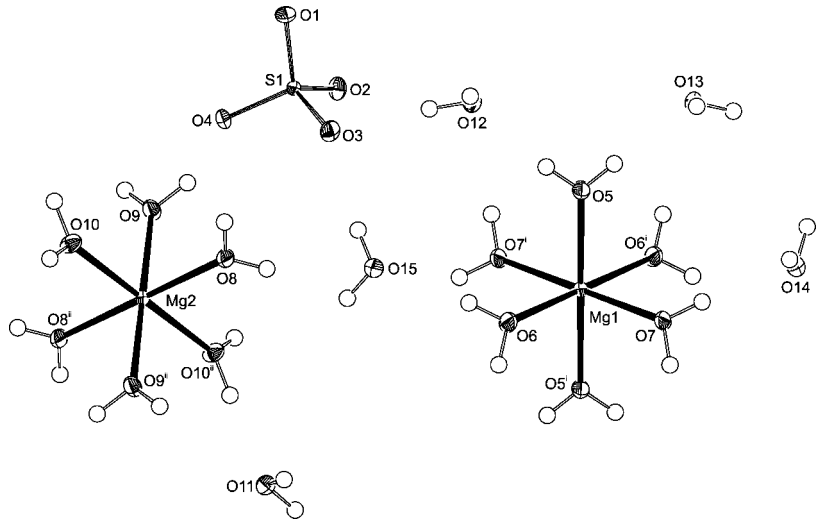


**Figure 4.** Displacement ellipsoid plot of $[Mg(H_2O)_6](SO_4)\cdot 5H_2O$, drawn at the 50% probability level. Symmetry operations i: $1-x, 1-y, 1-z$; ii: $1-x, 1-y, -z$.

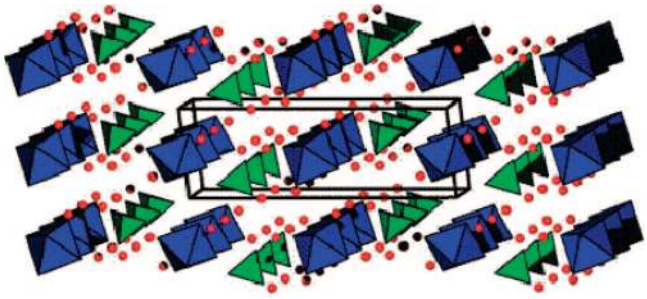

**Figure 5.** Packing of $[Mg(H_2O)_6](SO_4)\cdot 5H_2O$ in the crystal. Hydrogen atoms are omitted for clarity. The $Mg(H_2O)_6$ octahedra are drawn in blue, the sulfate tetrahedra are in green, and the uncoordinated water oxygen atoms are red spheres of arbitrary radii.

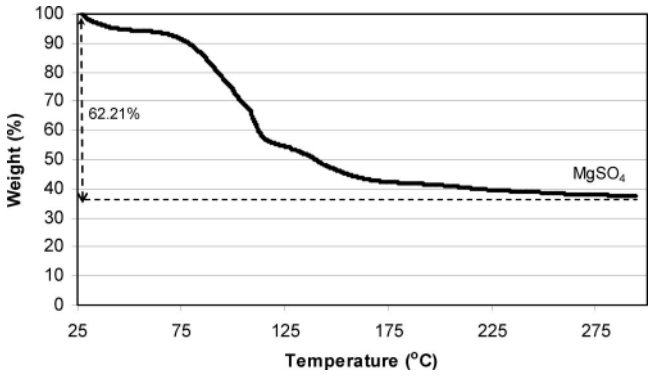


**Figure 6.** TGA curve of $MgSO_4\cdot 11H_2O$.

to 990 $cm^{-1}$ for $MgSO_4\cdot 11H_2O$. $MgSO_4\cdot 11H_2O$ has additional sulfate modes at 1116 and 1071 $cm^{-1}$.[34] Sulfate related Raman bands for $MgSO_4\cdot 7H_2O$ has a different Raman pattern with maxima at 1139, 1101, and 1067 $cm^{-1}$.

For $MgSO_4\cdot 11H_2O$, a water bending mode[34] is observed between 409 and 490 $cm^{-1}$ having a maximum at 444 $cm^{-1}$ and a sulfate mode between 585 and 680 $cm^{-1}$ with a maximum at 620 $cm^{-1}$. For $MgSO_4\cdot 7H_2O$, the same bands for water and sulfate can be observed and are located between 418 and 496 $cm^{-1}$ having a maximum at 455 $cm^{-1}$ and in the range of 566–668 $cm^{-1}$, having a maximum at 618 $cm^{-1}$, respectively.

Raman bands reported at 379 $cm^{-1}$ for Mg−O[34] vibrations of $MgSO_4\cdot 7H_2O$ are not present in the spectrum of $MgSO_4\cdot 11H_2O$ in Figure 7.

The bands at 255 and 177 $cm^{-1}$ for $MgSO_4\cdot 7H_2O$ are close to the frequency values observed in the literature,[35] and have been assigned to O−H···O (sulfate) entities in the crystal structure (255 $cm^{-1}$), and to O−Mg−O deformations, respectively. For $MgSO_4\cdot 11H_2O$, the O−H···O (sulfate) vibration is located at lower energies (233 $cm^{-1}$) than those given in the literature for $MgSO_4\cdot 7H_2O$ (255 $cm^{-1}$), most likely due to the presence of additional lattice–water. On the contrary, the corresponding O−Mg−O band for $MgSO_4\cdot 11H_2O$ seems to be shifted to a higher wavenumber, that is, 190 $cm^{-1}$.

The stretching modes of water incorporated in the lattice are located in the 2900–3700 $cm^{-1}$ region. For $MgSO_4\cdot 11H_2O$, there seems to be one dominant band having a maximum at 3395 $cm^{-1}$, with potential shoulders at 3520, 3300, and 3150 $cm^{-1}$. For $MgSO_4\cdot 7H_2O$, two bands are resolved at 3427 and 3325 $cm^{-1}$, including a shoulder at 3212 $cm^{-1}$. The bands located at 1669 $cm^{-1}$ for $MgSO_4\cdot 11H_2O$ and at 1678 $cm^{-1}$ for $MgSO_4\cdot 7H_2O$ can be assigned to bending modes of intracrystalline water.[36]

Summarizing, by comparing the vibrational spectra of the $MgSO_4\cdot 11H_2O$ and $MgSO_4\cdot 7H_2O$ salts, it can be concluded that significant differences exist in the type of interactions of water with sulfate groups in the lattice, in view of the different O−H stretching vibrations, as well as sulfate, O−H···O (sulfate), and O−Mg−O bands vibrational modes.

It should be noted that the Raman spectrum of $MgSO_4\cdot 11H_2O$ is very similar to the spectra of a salt found as inclusions denoted as $MgSO_4\cdot 12H_2O$ but presumably the undecahydrate form in Holocene ice cores from Dome Fuji-East Antarctica.[37] The strongest $SO_4^{2-}$ band is in both cases located at 989 $cm^{-1}$ (symmetrical stretching mode), including the weaker modes maximizing at 1117 and 1071 $cm^{-1}$. This suggests that micro inclusions of $MgSO_4$ salt preserved inside ice cores at low temperature to some extent contain $MgSO_4\cdot 11H_2O$ salt.

Natural occurrence of $MgSO_4\cdot 11H_2O$ crystals has been found in sea ice inclusions from Saroma Lake-Japan, recognized as a valid mineral by International Mineralogical Association (IMA) Commission, and named "meridianiite". The existence of meridianiite mineral in sea ice has been proven by showing the

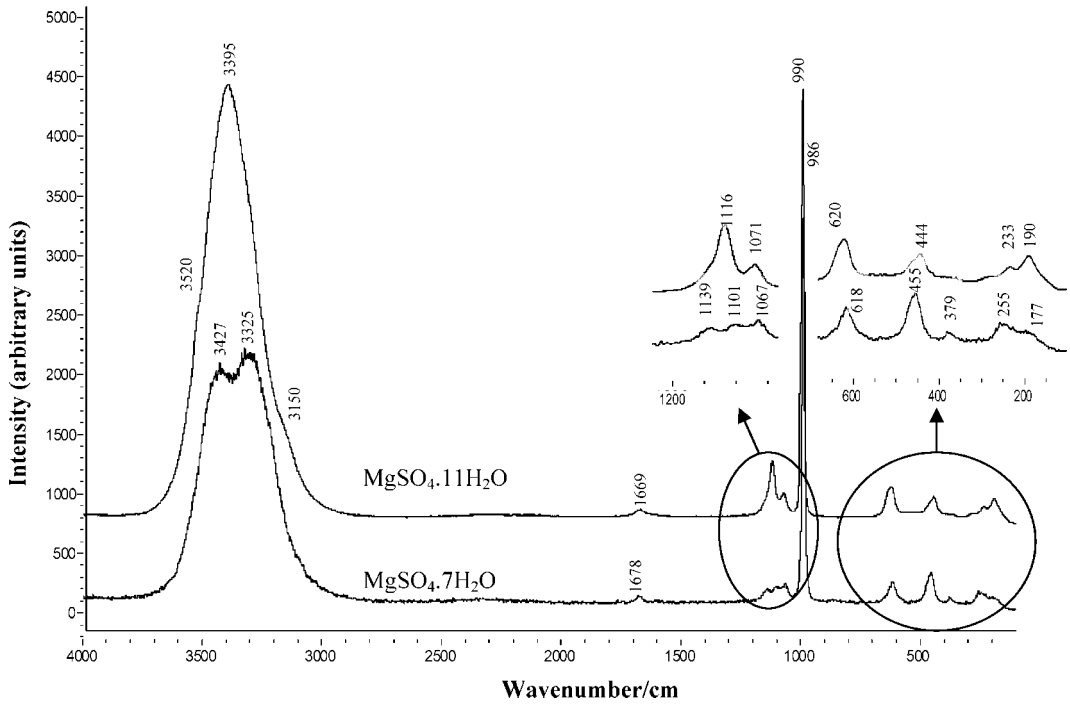


**Figure 7.** Raman spectra of $MgSO_4 \cdot 11H_2O$ and $MgSO_4 \cdot 7H_2O$ crystals.

excellent micro Raman spectra vibrational harmony between the synthetic $MgSO_4 \cdot 11H_2O$ and the inclusions in the sea ice sample.[38]

**Molecular Modeling.** On the basis of XRD data, single crystal structure and cell parameters were determined. The morphology module of Cerius$^2$ v.3.9 (Accelys) was used to determine the BFDH morphology[39] (in vacuum) shown in Figure 2e. Measuring the angles between the faces in the crystals, a suggestion for face indexing of the experimental morphology in Figure 2d is given in Figure 2f. The experimental (2d, 2f) 110 and $\bar{1}\bar{1}0$ faces grow slightly slower than 010 and $0\bar{1}0$, probably due to solvent effects. The 001 face is dominant both in the BFDH and experimental morphology.

**Inclusions.** Small pockets of mother liquor (inclusions) are visible in the interior of the crystal in Figure 2c. Inclusions develop during the course of crystal growth.[40] These inclusions show as negative crystals (mother liquor inclusions bounded by the crystal faces of that crystal) which have a morphology similar to the $MgSO_4 \cdot 11H_2O$ crystal. Under isothermal conditions inclusion may change shape or unite as the internal system adjusts itself toward the condition of minimum surface energy.[41] It is proposed that the large inclusions (negative crystals) result from the formation of liquid parent inclusions and the subsequent inward growth and coalescence during long storage of the crystals.[42] The inclusions vary in size from 50 to 200 $\mu$m.

## Conclusion

This paper corrects the misconception in the literature for $MgSO_4 \cdot 11H_2O$ crystals mistakenly labeled $MgSO_4 \cdot 12H_2O$ by Fritzsche in 1837. $[Mg(H_2O)_6](SO_4) \cdot 5H_2O$ ($MgSO_4 \cdot 11H_2O$), was grown from magnesium sulfate solution by eutectic freezing and by cooling crystallization around eutectic conditions. Single crystal XRD studies were carried out at a temperature of 110(2) K, and crystal structure [triclinic with space group $P\bar{1}$ (No. 2)] and cell parameters $a = 6.72548(7)$ Å, $b = 6.77937(14)$ Å, $c = 17.2898(5)$ Å, $\alpha = 88.255(1)°$, $\beta = 89.478(2)°$, $\gamma = 62.598(1)°$, $V = 699.54(3)$ Å$^3$, $Z = 2$ were calculated. Thermogravimetric analysis proved the stochiometry of the $MgSO_4 \cdot 11H_2O$ salt. The corrected phase diagram of $MgSO_4$ for the range 17.3–21.4%-w $MgSO_4$ and temperature $-3.9$ to $+1.8$ °C is given. The Raman spectrum of $MgSO_4 \cdot 11H_2O$ showed significant differences with that of $MgSO_4 \cdot 7H_2O$. The natural occurrence of $MgSO_4 \cdot 11H_2O$ in sea ice inclusions from Saroma Lake-Japan, its recognition by IMA as a mineral, and its name (meridianiite) has been announced. The Miller indices of $MgSO_4 \cdot 11H_2O$ crystals are also presented. Negative crystals, formed in inclusions, exhibited the same morphology.

**Acknowledgment.** This work was supported by the EET (Energy, Ecology and Technology) program of the Ministries of Economic Affairs, VROM, O&W and Kemira, Nedmag, Larox-Pannevis, TNO, DSM and was also supported (M.L., A.L.S.) by the Council for Chemical Sciences of The Netherlands Organization for Scientific Research (CW-NWO). We would also like to thank Dr. Joop Ter Horst for morphology prediction, Hirokazu Shibata and Dr. Guido Mul for Raman spectroscopy, and Duco Bosma for TGA measurements.

**Supporting Information Available:** Crystallographic files in CIF format are available free of charge via the Internet at http://pubs.acs.org.

## References

(1) Gmelin, *Gmelins Handbuch der Anorganischen Chemie*; Verlag Chemie: Weinheim, 1958.
(2) Baur, W. H. *Acta Crystallogr.* **1964**, *17*, 1361–1369.
(3) Ramalingom, S.; Podder, J.; Narayana Kalkura, S. *Cryst. Res. Technol.* **2001**, *36* (12), 1357–1364.
(4) Zalkin, A.; Ruben, H.; Templeton, D. H. *Acta Crystallogr.* **1964**, *17*, 235–240.
(5) Aleksovska, S.; Petrusevski, V. M.; Soptrajanov, B. *Acta Crystallogr.* **1998**, *B54*, 564–567.
(6) Himawan, C.; Kramer, H. J. M.; Witkamp, G. J. *Sep. Purif. Technol.* **2006**, *50*, 240–248.
(7) Genceli, F. E.; Gaertner, R. S.; Witkamp, G. J. *J. Cryst. Growth* **2005**, *275* (1–2), e1369–e1372.
(8) Marion, G. M.; Farren, R. E. *Geochim. Cosmochim. Acta* **1999**, *63* (9), 1305–1318.

(9) Pillay, V.; Gaertner, R. S.; Himawan, C.; Seckler, M. M.; Lewis, A. E.; Witkamp, G. J. *J. Chem. Eng. Data* **2005**, *50* (2), 551–555.
(10) Smits, A.; Rinse, J.; Koymans, L. H. *Z. Phys. Chem. Abt. Anorgan. Chem.* **1928**, *135*, 78–84.
(11) Meyer, J.; Aulich, W. *Z. Anorg. Chem.* **1928**, *127*, 329.
(12) Hogenboom, D. L.; Kargel, J. S.; Ganasan, J. P.; Lee, L. *Icarus* **1995**, *115*, 258–277.
(13) Chernogorenko, V. B. *Zh. Neorg. Khim.* **1956**, *I*, 317–322.
(14) Fritzche, C. J. *Pogg. Ann.* **1837**, *42*, 577–580.
(15) Van't Hoff, J. H.; Meyerhoffer, W.; Smith, N. *Sitzungsberichte der Königlich Preussischen Akadem.* **1901**, 1034–1044.
(16) Kargel, J. S. *Icarus* **1991**, *94*, 368–390.
(17) Kajiwara, K.; Yabe, K.; Hashitani, T. *CryoLetters* **2003**, *24*, 143–148.
(18) Genceli, F. E.; Himawan, C.; Witkamp, G. J. *J. Cryst. Growth* **2005**, *275* (1–2), e1757–e1762.
(19) Genceli, F. E.; Trambitas, D. O.; Gärtner, R. S.; Rodriguez, M.; Witkamp, G. J. *VDI Berichte (1901 II)* **2005**, 855–860.
(20) Himawan, C. Characterization and Population Balance Modelling of Eutectic Freeze Crystallization, Ph.D. Dissertation, Delft University of Technology, The Netherlands, 2005.
(21) Gaertner, R. S.; Genceli, F. E.; Trambitas, D. O.; Witkamp, G. J. *J. Cryst. Growth* **2005**, *275* (1–2), e1773–e1778.
(22) Duisenberg, A. J. M.; Kroon-Batenburg, L. M. J.; Schreurs, A. M. M. *J. Appl. Crystallogr.* **2003**, *36*, 220–229.
(23) Sheldrick, G. M. *SADABS: Area-Detector Absorption Correction*, *v2.10*; Universität Göttingen, Germany, 1999.
(24) Sheldrick, G. M. *SHELXS-97: Program for Crystal Structure Solution*; Universität Göttingen, Germany, 1997.
(25) Sheldrick, G. M. *SHELXL-97: Program for Crystal Structure Refinement*; Universität Göttingen, Germany, 1997.
(26) Spek, A. L. *J. Appl. Crystallogr.* **2003**, *36*, 7–13.
(27) Bock, C. W.; Kaufman, A.; Glusker, J. P. *Inorg. Chem.* **1994**, *33*, 419–427.
(28) Pilati, T.; Forni, A. *J. Appl. Crystallogr.* **1998**, *31*, 503–504.
(29) McIntyre, G. J.; Ptasiewicz-Bak, H.; Olovsson, I. *Acta Crystallogr.* **1990**, *B46*, 27–39.
(30) Schomaker, V.; Trueblood, K. N. *Acta Crystallogr.* **1986**, *B24*, 63–76.
(31) Calleri, M.; Gavetti, G.; Ivaldi, G.; Rubbo, M. *Acta Crystallogr.* **1984**, *B40*, 218–222.
(32) Lutz, M.; Spek, A. L. *private communication*, 2005.
(33) Batsanov, A. S. *Acta Crystallogr.* **2000**, *C56*, e230–e231.
(34) Makreski, P.; Jovanovski, G.; Dimitrovska, S. *Vib. Spectrosc.* **2005**, *39*, 229–239.
(35) Parsk, H. J.; Boutin, H. *J. Chem. Phys.* **1966**, *45*, 3284.
(36) Socrates, G. *Infrared and Raman Characteristic Group Frequencies-Tables and Charts*, 3rd ed.; John Wiley & Sons: New York, 2001.
(37) Ohno, H.; Igarashi, M.; Hondoh, T. *Earth Planet. Sci. Lett.* **2005**, *232*, 171–178.
(38) Genceli, F. E.; Horikawa, S.; Iizuka, Y.; Sakurai, T.; Hondoh, T.; Kawamura, T.; Witkamp, G. J. *J. Glaciol.* submitted.
(39) Van der Eerden, J. P.; Bruinsma O. S. L. *Science and Technology of Crystal Growth*; Kluwer Academic Publishers: Norwell, MA, 1995.
(40) Mullin J. W. *Crystallization*, 4th ed.; Elsevier: Amsterdam, 2001.
(41) Denbigh, K. G.; White, E. T. *Chem. Eng. Sci.* **1966**, *21*, 739–754.
(42) Hu, X. B.; Jiang, S. S.; Huang, X. R.; Zeng, W.; Lui, W. J.; Chen, C. T.; Zhoa, Q. L.; Jiang, J. H.; Wang, Y. L.; Tian, Y. L.; Han, Y. *J. Cryst. Growth* **1996**, *163*, 266–271.

CG060794E